

EVAPORATION OF COMPACT YOUNG CLUSTERS NEAR THE GALACTIC CENTER

Sungsoo S. Kim

Department of Physics, Korea Advanced Institute of Science & Technology, Daejeon 305-701, Korea

Mark Morris

*Department of Physics & Astronomy, University of California, Los Angeles, CA 90095-1562;
Institut d'Astrophysique de Paris, 98 bis Bvd. Arago, 75014 Paris, France*

Hyung Mok Lee¹

Department of Astronomy, Seoul National University, Seoul 151-742, Korea

ABSTRACT

We investigate the dynamical evolution of compact young clusters (CYCs) near the Galactic center (GC) using Fokker-Planck models. CYCs are very young (< 5 Myr), compact (< 1 pc), and only a few tens of pc away from the GC, while they appear to be as massive as the smallest Galactic globular clusters ($\sim 10^4 M_\odot$). A survey of cluster lifetimes for various initial mass functions, cluster masses, and galactocentric radii is presented. Short relaxation times due to the compactness of CYCs, and the strong tidal fields near the GC make clusters evaporate fairly quickly. Depending on cluster parameters, mass segregation may occur on a time scale shorter than the lifetimes of most massive stars, which accelerates the cluster's dynamical evolution even more. When the difference between the upper and lower mass boundaries of the initial mass function is large enough, strongly selective ejection of lighter stars makes massive stars dominate even in the outer regions of the cluster, so the dynamical evolution of those clusters is weakly dependent on the lower mass boundary. The mass bins for Fokker-Planck simulations were carefully chosen to properly account for a relatively small number of the most massive stars. We find that clusters with a mass $\lesssim 2 \times 10^4 M_\odot$ evaporate in $\lesssim 10$ Myr. Two CYCs observed near the GC — the “Arches cluster” (G0.121+0.17) and the “Quintuplet cluster” (AFGL2004) — are interpreted in terms of the models; their central densities and apparent ages are consistent with the hypothesis that they represent successive stages of cluster evolution along a common track, with both undergoing rapid evaporation. A simple calculation based on the total masses in observed CYCs and the lifetimes obtained here indicates that the massive CYCs comprise only a fraction of the star formation rate (SFR) in the inner bulge estimated from Lyman continuum photons and far-IR observations. This is consistent with the observation that many stars in the inner bulge form outside the large clusters.

Subject headings: celestial mechanics, stellar dynamics — Galaxy: center — methods: numerical — galaxies: star clusters

Accepted for publication in ApJ

¹This study was initiated when he was at Pusan National University, Dept. of Earth Sciences, Korea.

1. INTRODUCTION

The inner few hundred pc of the Galactic bulge (the inner bulge) contains stars of a variety of ages, in addition to an apparently coeval population of galactic-age stars. The evidence for recent massive star formation there has grown with the observations of several clusters of emission-line stars in that region. Intermediate-age stars have also been observed in the inner bulge in the form of OH/IR stars (Lindqvist, Habing, & Winnberg 1992; Sjouwerman et al. 1998). Noting the presence of these young and intermediate-age stars, Serabyn & Morris (1995) argued that star formation in the central molecular zone occupying the inner bulge has been sustained over the lifetime of the Galaxy in spite of the inhospitality of that environment for star formation, owing to large gas temperatures and turbulent velocities, strong magnetic fields, and strong tidal forces.

About half a dozen distinct sites of recent star formation have been found in the inner bulge, most notably including the “Arches cluster” (G0.121+0.017; Nagata et al. 1995; Cotera et al. 1996; Serabyn, Shupe, & Figer 1998) and the “Quintuplet cluster” (AFGL2004; Okuda et al. 1990; Nagata et al. 1990; Glass, Moneti, & Moorwood 1990; Figer, McLean, & Morris 1995, 1999), both lying within ~ 35 pc, in projection, of the Galactic center (GC). These clusters are very young (< 5 Myr), and compact (< 1 pc), while they appear to be as massive as the smallest Galactic globular clusters ($\sim 10^4 M_\odot$). Their young ages are manifested by the presence of ample massive stars: the Arches and Quintuplet contain about 120 and 30 stars having initial mass larger than $20 M_\odot$, respectively (Serabyn et al. 1998; Figer et al. 1999). Morris (1993) suggested that the non-standard star formation environment near the GC may lead to an initial mass function (IMF) skewed toward relatively massive stars (flatter IMF) and having an elevated mass cutoff. However, the observational limit for the lowest mass in these clusters is still as high as several M_\odot , so not much is known about the lower end of their mass function.

The Arches and Quintuplet clusters are two members of what appears to be a special category of clusters; indeed, their large masses place them at the lower end of the category of super star clusters (e.g., Ho & Filippenko 1996). Another known, potential member of this category near the GC is the young cluster in the central parsec, but because of its un-

usual location at the bottom of the Galactic gravitational potential well, and in the immediate vicinity of the central supermassive black hole, it may have had quite a different origin. Thus, it is not clear that this cluster should be categorized alongside the Arches and Quintuplet, even though it has a comparable mass (Figer et al. 1999). In any case, the calculations presented in this paper do not apply to the central cluster. The stellar cluster in Sgr B2 is potentially another supercluster currently in formation (e.g., Gaume et al. 1995), although it is not yet clear whether it will attain the status of the two more evolved clusters.

With the observations of these compact, young clusters (CYCs) near the GC, a natural question arises: Why don’t we observe older examples of CYCs? Are we witnessing very unusual events that happened to have recently taken place in the GC, or are older clusters rare because they evaporate in a relatively short period of time? The proximity of the CYCs to the GC implies a strong tidal field, and the short relaxation time due to their compactness makes very massive stars play an important dynamical role through mass segregation, which accelerates the dynamical evolution even more, before these stars disappear with mass loss and explosions. These two characteristics suggest fairly short lifetimes for the CYCs. The ages of the Arches and Quintuplet clusters are estimated to differ by about a factor of two, providing an excellent opportunity to compare observations with the numerical study of their dynamical evolution. Because their rather extreme parameters have only recently been recognized, these clusters have not yet been numerically and theoretically explored. In the present study, we investigate the clusters’ lifetime, t_{ev} , for various parameters plausible for CYCs, and compare the results with current observations of CYCs and with estimates of the star formation rate in the inner bulge.

A discussion of the time scales related to the dynamical evolution of spherical stellar systems and on our choice of simulation methods is given in § 2. We describe the details of our models in § 3, and show the simulation results in § 4. The implications of our results are discussed in § 5, and § 6 summarizes our findings.

2. BACKGROUNDS

2.1. Time Scales

The dynamical evolution of stellar systems is affected by many factors such as galactic tidal fields, the stellar mass function, and stellar evolution, as well as their overall mass and physical extent. In general, a cluster loses its mass by two-body relaxation and stellar evolution (via supernovae and stellar winds), and the resulting dynamical evolution of the cluster is accelerated by the presence of a strong tidal field.

The evolution of star clusters in a static tidal field has been studied extensively. Hénon (1961) obtained a self-similar solution for an expanding cluster assuming that there is a central energy source (which he speculated to be binaries). Such a cluster is found to evaporate completely in 22.5 times the half-mass relaxation time, which is defined as

$$t_{rh} = 0.138 \frac{M^{1/2} R_h^{3/2}}{\bar{m} G^{1/2} \ln \Lambda}, \quad (1)$$

where M is the total mass of the cluster, R_h the half-mass radius, \bar{m} the mean mass of each star, and G the gravitational constant. The $\ln \Lambda$ term appears because of the finite size of the cluster, and is called the Coulomb logarithm.

The numerical integration of the Fokker-Planck equation by Lee & Ostriker (1987) confirmed Hénon's general result. These works have been extended to multi-mass models for typical globular cluster parameters by Lee, Fahlman, & Richer (1991) and Lee & Goodman (1995), and the lifetimes of the clusters in units of half-mass relaxation time have been found to be shorter than those of single mass models by about a significant factor. Thus, clusters with a realistic mass function would survive less than 10 t_{rh} .

The evaporation of stars from the cluster is due to relaxation, but it takes some time for a star to escape from the cluster. Since this "lingering time" is of order of an orbital period of the star, the evaporation of a cluster depends on both relaxation time and dynamical time. The average orbital time scale for stars in the cluster can be expressed as:

$$t_{dyn} \approx \left(\frac{R_t^3}{GM} \right)^{1/2}, \quad (2)$$

where R_t is the tidal radius of the cluster,

$$R_t = \left(\frac{M}{2M_g} \right)^{1/3} R_g. \quad (3)$$

Here, R_g is the galactocentric radius, and M_g the enclosed galactic mass within R_g . Equations (1) and (2) give a relation $t_{dyn}/t_{rh} \propto N^{-1}$, where N is the number of stars. Thus the evaporation depends more sensitively on N when N is small. Note that since M_g is a function of R_g (see eq. [4]), equations (2) and (3) imply that t_{dyn} can be expressed in terms of R_g only.

Stellar evolution affects a cluster's dynamical evolution in several ways. First, mass loss by stellar evolution (through stellar winds and explosions) itself accelerates the mass loss of a cluster and thus shortens the cluster's lifetime. Furthermore, the mass loss by stellar evolution, together with tidal evaporation, may prevent the core collapse. Since stars bound to a cluster have negative energy and massive stars are predominantly located in the core due to mass segregation, the mass loss from the cluster thus has an indirect heating effect.

The effect of very massive stars may be neglected for globular clusters, which have initial t_{rh} of $\sim 10^9$ – 10^{10} yr, much longer than evolutionary time scales of high mass stars. The low mass stars eventually undergo evolution on a much longer time scale, and their effects on dynamics should be very small. Therefore, in old globular clusters, the stellar evolution should have been effective only in the initial phase when the relaxation did not play any role. The subsequent evolution should have been governed mostly by the relaxation process alone. Thus the study of globular cluster evolution may assume that clusters start with upper mass boundary, m_u , much lower than the real initial value (for example, for m_u , Chernoff & Weinberg 1990 adopted $15 M_\odot$ with stellar evolution, and Lee, Fahlman, & Richer 1991 adopted $0.8 M_\odot$ without stellar evolution). However, the sizes of CYCs near the GC are very small for their masses, leading to initial t_{rh} as short as $\sim 10^6$ – 10^7 yr. Moreover, the mass segregation time, $t_{rh} \bar{m}/m_u$, may be even shorter than the lifetime of the most massive star. Then very massive stars play an important role in the evolution of the cluster through rapid mass segregation and subsequent demise.

To summarize, the dynamical evolution of a cluster is determined by relative differences between time scales for the above processes, two-body relaxation including core collapse and subsequent expansion, tidal evaporation, stellar evolution, and mass segregation. For example, stellar evolution determines the cluster evolution time scale when the chemical evolution of massive stars occurs much faster than the relaxation

time scale of the cluster, and the relaxation governs the cluster evolution when its time scale is shorter than that of stellar evolution. Also, if a cluster has a large stellar mass range, the segregation of massive stars toward the central parts shortens the relaxation time in the core and makes relaxation processes more important. Finally, a strong tidal field accelerates all these processes. Since the time scales of these processes scale with cluster parameters in different ways, scaling the evolutionary route of one cluster to another is quite limited, and numerical simulations are generally required for the unexplored parameter regime.

2.2. N-body vs. Fokker-Planck Models

For the study of dynamical evolution of spherical stellar systems, N-body and Fokker-Planck simulations are among the most widely used methods. The N-body method is certainly more realistic and requires less assumptions than other methods, but real-number N-body simulations for CYCs having $N \sim 10^3\text{--}5$ are still prohibitively expensive in terms of computing time, especially in the context of a simulation survey in which a range of parameters is being explored. Many studies based on the N-body method use a time-scaling technique to simulate a large-number system with a smaller number of stars on behalf of computing cost. However, correct scaling is not always guaranteed when the stellar evolution time scale, t_{se} , is not well separated from t_{dyn} and t_{rh} , as might be the case of CYCs (see, however, Aarseth & Heggie 1998 for a compromise technique, “variable scaling”). Also, as mentioned above, the evaporation rate of tidally-limited clusters is a function of both t_{rh} and t_{dyn} , which scale differently with N and M . Thus, direct N-body calculations of the system with a smaller number of stars are not able to correctly mimic the evaporation of the system with a larger N . Moreover, when the mass function is steep, the upper mass boundary, m_u , can be a function of the total number of stars in the cluster for statistical reasons (the more stars, the higher m_u). Then the system with a smaller number could not properly represent the full mass range of the larger system.

On the other hand, although the Fokker-Planck method requires more assumptions and approximations, it is much less expensive and gives statistically correct results. These features are critically beneficial, not only when the study is meant for a parameter survey, but also when statistically stable results with-

out random noise are necessary for theoretical analyses. For these reasons, as a first step of our study of the fate of CYCs, we simulate the dynamical evolution of CYCs using Fokker-Planck models. We are planning N-body simulations for a few representative cluster parameter sets in a followup study.

A recent comparison between Fokker-Planck and N-body simulations for tidally-limited clusters showed a discrepancy in cluster lifetime between the two methods (Fukushige & Heggie 1995; Portegies Zwart et al. 1998). However, Takahashi & Portegies Zwart (1998) were able to show that this discrepancy can be successfully removed by adopting anisotropic Fokker-Planck models with the “apocenter criterion” and an appropriate constant for the speed of star removal behind the tidal radius. Here we adopt anisotropic Fokker-Planck models and the apocenter criterion as an effort to minimize the possible discrepancy with N-body simulations.

3. MODELS

We have used the two-dimensional (energy-angular momentum space), orbit-averaged Fokker-Planck code by Takahashi (1997). The code assumes that star clusters are spherically symmetric and are in dynamical equilibrium.

For our initial models, we adopt a multi-mass distribution function composed of single mass King models with equal velocity dispersions. It is assumed that clusters initially fill the tidal radius and that all stars in the cluster are formed simultaneously at $t = 0$. The relation between M and R_t is determined via equation (3) and

$$M_g = 2 \times 10^8 M_\odot \left(\frac{R_g}{30 \text{ pc}} \right)^{1.2}, \quad (4)$$

which was adopted from Genzel & Townes (1987). Primordial binaries are not considered in this study, and the Coulomb logarithm is taken as $\ln \Lambda = \ln N$.

Heating by binaries formed through three-body processes and tidal-capture processes is included. For the heating rate per unit volume by three-body binaries, we adopt the formulation by Lee et al. (1991):

$$\dot{E}_{3b} = 4.21 \times 10^3 G^5 \left(\sum_i \frac{n_i m_i^2}{v_i^3} \right)^3 v_c^2, \quad (5)$$

where the summation is over all mass components, n_i and v_i^2 are the number density and velocity dispersion of component i , respectively, and v_c^2 is the

mass-weighted, central velocity dispersion. On the other hand, we use a modified version of the tidal-capture binary heating rate per unit volume by Lee & Ostriker (1993):

$$\dot{E}_{tc} = \sum_i \sum_{j \geq i} (m_i + m_j + \bar{m}_c) \sigma_{tc} v_{ij} n_i n_j \phi_c, \quad (6)$$

where the summation i is only for main-sequence stars, \bar{m}_c is the mean mass in the center, σ_{tc} the tidal-capture cross section, v_{ij} the relative rms velocity between components i and j , and ϕ_c the central gravitational potential. The fitting formulae of Kim & Lee (1999) were adopted for σ_{tc} .

The effect of the Galactic tidal field is assumed to be constant (circular orbit around the GC and spherically symmetric potential due to the tidal force) and is realized by imposing a tidal boundary. A star is removed if its apocenter distance, R_a , exceeds the tidal radius, R_t (apocenter criterion; Takahashi, Lee, & Inagaki 1997). Removal of stars satisfying the apocenter criterion is realized by the formalism of Lee & Ostriker (1987):

$$\frac{df}{dt} = -\alpha_{esc} f \left[1 - \left(\frac{E}{E_t} \right)^3 \right]^{1/2} \frac{1}{2\pi} \sqrt{\frac{4\pi}{3}} G \rho_t, \quad (7)$$

where f is the distribution function, E_t the tidal energy, and ρ_t the mean mass density within the tidal radius. This formula accounts for the persistence time of an escaping star, and the speed of star removal is determined by a dimensionless constant α_{esc} . Following Takahashi & Portegies Zwart (1998), we have adopted $\alpha_{esc} = 2$.

The effect of stellar evolution is realized by secularly decreasing the mass of each component. Following Chernoff & Weinberg (1990), the mass of each component is linearly decreased by

$$m_i(t) = m_i(0) - [m_i(0) - m_{i,f}] \frac{(t - \tau_{i+\frac{1}{2}})}{(\tau_{i-\frac{1}{2}} - \tau_{i+\frac{1}{2}})} \quad \text{for } \tau_{i+\frac{1}{2}} < t < \tau_{i-\frac{1}{2}}, \quad (8)$$

where $m_i(t)$ is the mass of component i at time t , $m_{i,f}$ the final mass of the component, $\tau_{i \pm \frac{1}{2}}$ the lifetime of a star with mass $m_{i \pm \frac{1}{2}}$ (see below for $m_{i \pm \frac{1}{2}}$). For $t < \tau_{i+\frac{1}{2}}$, $m_i(t)$ has a constant value of $m_i(0)$, and for $t > \tau_{i-\frac{1}{2}}$, $m_i(t)$ is set to $m_{i,f}$. For intermediate and low mass stars, the mass evolution between the main-sequence and degenerate stage is so abrupt that it can

be approximated with a step function. However, in case of massive stars ($m > 20 M_\odot$), the mass evolution is continuous throughout the stellar lifetime, so it is quite difficult to define the time for which a star maintains its initial mass and after which the star becomes degenerate. Furthermore, it is not trivial to implement such continuous mass loss into a mass component which is a representation of a set of stars with a certain range of masses and mass loss rates. For this reason, here we define an ‘‘effective lifetime’’ of a star such that

$$\tau_{eff} = \frac{1}{m(0)} \int_0^{t_f} m(t) dt, \quad (9)$$

where $m(t)$ is the mass evolution of a star with initial mass $m(0)$, t_f is the time required for the mass of a star with initial mass $m(0)$ to become the final mass m_f . We have adopted Schaller et al. (1992) for $m(t)$ and t_f , and Drukier (1995) for m_f . Figure 1 is a plot of τ_{eff} as a function of $m(0)$ obtained in this way. Then this τ_{eff} is used for $\tau_{i \pm \frac{1}{2}}$ in equation (8).

The mass spectrum is represented by a set of discrete mass components. For the mass binning, equal logarithmic space binning has been used in many previous studies. However, the same logarithmic binning is not appropriate for representing largely different mass spectrum slopes at the same time. In particular, the logarithmic binning may result in too small number of stars for the most massive bins of a cluster with steep mass spectrum and/or with small M , which is not desirable for Fokker-Planck models. One could lower the upper mass boundary in accordance with the cluster parameters to avoid such a problem, but then the problem becomes how one ‘‘decides’’ the upper mass boundary. Generally, one is interested in a cluster with given M , α , and m_l . In cases where the relaxation time of a cluster is much longer than the stellar evolution time for massive stars, the effect of those massive stars on the dynamical evolution of the cluster may be neglected and the choice of m_u is relatively unimportant. However, in case of our target clusters, the role of massive stars is expected to be important because of their short relaxation times, and thus m_u should be chosen carefully. For this reason, we bin the mass in a way that guarantees all mass components to have the number of stars larger than a certain minimum value. The mass range is binned to make all components have equal value of

$$\int_{m_{i-\frac{1}{2}}}^{m_{i+\frac{1}{2}}} m^\beta N(m) dm, \quad (10)$$

where $[m_{i-\frac{1}{2}}, m_{i+\frac{1}{2}}]$ is the mass range of a component i . Thus the mass ranges of each component differ for models with different parameters. For a given M , m_u , m_l , α , and N_{bin} (number of bins), one can determine the value of β that assigns a stellar number of N_u to the most massive bin. Once β is determined, $m_{i\pm\frac{1}{2}}$ is obtained by equation (10) with given m_l and m_u . Here we adopted $m_u = 150 M_\odot$, $m_l = 0.1, 1 M_\odot$, $N_{bin} = 15$, and $N_u = 50$. In this way, the effects of the most massive stars can be realized in Fokker-Planck models correctly and consistently. Note that $\beta = 1$ is for equal mass binning, and $\beta = 0$ is for equal number binning.

We choose the initial mass spectrum to be a simple power law

$$dN(m) \propto m^{-\alpha} dm, \quad (11)$$

where $dN(m)$ is the initial number of stars with masses between m and $m + dm$, and $\alpha = 2.35$ gives a Salpeter initial mass function. The initial mass of component i , $m_i(0)$, is calculated by

$$m_i(0) = \frac{\int_{m_{i-\frac{1}{2}}}^{m_{i+\frac{1}{2}}} m^{1-\alpha} dm}{\int_{m_{i-\frac{1}{2}}}^{m_{i+\frac{1}{2}}} m^{-\alpha} dm}, \quad (12)$$

and the initial total mass of component i is

$$M_i(0) = \int_{m_{i-\frac{1}{2}}}^{m_{i+\frac{1}{2}}} N(m)m dm \quad (13)$$

The number of stars in component i , N_i , is then defined to be M_i/m_i . In Table 1, β and the initial mass of the most massive component, $m_{15}(0)$, are given for all models. Note that β and m_{15} are determined by M , m_l , and α because we fix m_u , N_{bin} , and N_u .

4. RESULTS

An example of the cluster evolution in our models is shown in Figure 8. A mild core collapse takes place at ~ 0.6 Myr, and the postcollapse expansion is accelerated by indirect heating due to stellar evolution starting from ~ 2.2 Myr, which is clearly manifested by a rather abrupt change in R_t slope. The mildness of the core collapse is only an apparent phenomenon: the relative increase of ρ_c during the collapse becomes larger when ρ_c is plotted for only the most massive component. While the core collapse and postcollapse expansion time scales are determined by the size, structure, and mass function of the cluster,

the stellar evolution time scale is dependent only on the mass function. Since these time scales are comparable for most of our models, the lifetime of a cluster will be determined jointly by these time scales in a complex way. In this section, we discuss the effect of each cluster parameter on the evolution of the cluster. We pay special attention to t_{ev} , which is given in Table 1, since this is closely related to the fate of the cluster.

Most of the discussion of evaporation and dynamical evolution assumes that the time is expressed in units of relaxation time. That is useful if the relevant process is related mostly to the two-body relaxation time. However, the stellar evolution is important in the situation that we are considering here, as discussed in § 2.1. Therefore, it is more convenient to express the results in absolute time for the CYCs.

4.1. Initial Concentration (W_0)

King models, which we use as initial models, are a one-parameter family, whose parameter W_0 determines the initial degree of central concentration (the larger the value of W_0 , the higher the concentration). Figure 2 shows the evolution of models 101, 111, and 112, which have the same initial conditions except for W_0 . While the times to total evaporation t_{ev} are almost the same, the epochs of the central density peak for these three models are largely different. The time to core collapse, t_{cc} , is determined by the central relaxation time, t_{rc} , which is smaller for more concentrated clusters, while the tidal evaporation rate is determined by a cluster's global properties. Clusters slowly expand in the postcollapse phase, and this expansion accelerates the tidal evaporation. The evaporation times are nearly the same for these models because we required our models to have the same t_{dyn} (the same R_g), M , and R_t . The evaporation is not sensitive to the detailed structure of the cluster, but depends mainly on macroscopic parameters such as M and R_t . Thus the insensitivity of t_{ev} on W_0 will hold for the parameter regime covered by our other models as well. The evolution of the central parameters depends on W_0 just because the core collapse is determined by the local conditions in the center, which depend on the initial models.

4.2. Mass Range (m_l)

The effects of lower and upper mass boundaries on t_{ev} might be seen by comparing models 101, 102, and

103. One may expect that m_l is more important in determining t_{ev} than m_u because \bar{m} varies more with m_l than m_u for our α values. However, interestingly, the results of models 101 to 103 show the opposite behavior: t_{ev} is approximately proportional to m_{15}^{-1} , but is almost insensitive to m_l (see next subsection for the relation between t_{ev} and m_{15}). Generally, a cluster with a mass spectrum rearranges itself so that heavies dominate the central region of the cluster and lights the outer region in a time scale $\sim t_{rh}m_l/m_u$ ($\sim t_{rh}m_l/m_{15}$ in our case; m_{15} better represents the upper mass boundary than m_u does because m_{15} accounts for the mass spectrum; see §3). However, the mass ranges of the above models are so wide (thus the ratios m_{15}/m_l are large) that even the outer region is dominated by heavies. This can be clearly seen in the density profile plot (Figure 3), where heavier components are dominant throughout most of the cluster. This presumably results from the selective evaporation of lighter components due to equipartition. However, the dominance of heavies in the outer region does not solely explain the similar t_{ev} of models 101 and 102 because the masses of the light components of these models are largely different and may contribute to t_{rh} in dissimilar ways.

The postcollapse density profiles are not far from the profile at the end of the collapse, and the latter may be described by the empirical relations:

$$\rho_i(0) \propto B(3/2, p_i + 1)(-E_0)^{p_i + 3/2} \quad (14a)$$

$$\frac{d \ln \rho_i}{d \ln r} = -0.23(p_i + 3/2) \quad (14b)$$

$$\frac{p_i}{m_i} = \frac{p_u}{m_u} \quad (14c)$$

where subscripts i and u are for the i th component and the most massive component, respectively, $B(x, y)$ is the Beta function, and E_0 the central potential (Bahcall & Wolf 1977, Cohn 1985). The above relation stems from $f_i \propto (-E)^{p_i}$, which is an approximate distribution function that a cluster has during the collapse. Cohn found that $p_u \approx 8.2$. Equations (14a) and (14b) give nearly the same profiles for $p_i \ll 1$, which is seen also in Figure 3. Thus when a cluster has a wide mass range, its outer region is dominated by heavier components, and t_{rh} is not dependent on m_l as long as $m_l \ll m_u/8.2$ ($\ll m_{15}/8.2$ in our case). Such insensitivity of t_{rh} to m_l is also seen between models 113 & 115 (smaller α), models 111 & 117 (smaller W_0), models 112 & 118 (larger W_0), models 125 & 129 (smaller M), and models 122

& 127 (larger M). On the other hand, t_{ev} 's of models with $\alpha \geq 2.35$ do depend on m_l , especially for $M = 5 \times 10^3 M_\odot$ (see Figure 4). This is because their mass ranges $[m_l, m_{15}]$ are not wide enough.

4.3. Initial Mass Function (α)

We discuss the effect of α on t_{ev} in terms of m_{15} (recall that m_{15} is a function of α). Models 113, 101, 142, and 114 have the same M ($= 2 \times 10^4 M_\odot$) but different α values. As noted above, t_{ev} is inversely proportional to m_{15} (see Figure 5) because of the predominance of heavier components in determining t_{rh} after rapid mass segregation. Models 124, 125, 141, and 126 ($M = 5 \times 10^3 M_\odot$) show the same proportionality too.

Models 121, 122, 143, and 123 ($M = 10^5 M_\odot$; different α) do not exactly follow the $t_{ev} \propto m_{15}^{-1}$ relation (although there is still a clear inverse relation between t_{ev} and m_{15}). As a cluster's mass becomes larger, its lifetime and m_{15} increase, and therefore the stellar evolution timescale is a relatively smaller fraction of the cluster's lifetime, and the relative amount of mass that is subject to loss by stellar evolution before cluster evaporation becomes larger. Since the relative amount of mass that is subject to loss by stellar evolution in a given period is a function of α , t_{ev} is not simply proportional to m_{15}^{-1} for the more massive clusters in which the stellar evolution effect is not negligible.

4.4. Galactocentric Radius (R_g)

Without stellar evolution, clusters with the same M would evolve with a time scale proportional to $t_{rh} \propto R_t^{3/2} \propto R_g^{9/10}$ (see eqs. [1], [3], and [4]). However, the effect of stellar evolution on t_{ev} is important in many of our models, and the applicability of this relation is limited. Figure 6 shows t_{ev} of models with $\alpha = 2$ and 2.35 as a function of R_g and M . In case of $\alpha = 2$, the $t_{ev} \propto R_g^{9/10}$ relation holds only for the models with $M = 5 \times 10^3 M_\odot$, where models end before any significant stellar evolution, due to relatively low m_{15} values. Stellar evolution significantly affects t_{ev} of the other $\alpha = 2$ models, for which the exponent in the above relation is smaller than 9/10. For $\alpha = 2.35$ models, where the role of massive stars is relatively less important, the effect of stellar evolution is much less apparent. Models with $M \leq 2 \times 10^4 M_\odot$ end before stellar evolution has had a significant effect, and the slope of $\log t_{ev}$ over $\log R_g$ of models

with $M = 10^5 M_\odot$ is affected by stellar evolution only slightly.

5. DISCUSSION

5.1. Overview of the Results

Our t_{ev} survey results show that for our parameter regime, CYCs will evaporate in less than or about 10 Myr, except for some cases with $M = 10^5 M_\odot$ and $\alpha \geq 2.35$. The compactness of CYCs, strong tidal fields, and large stellar mass ranges are jointly responsible for the short lifetimes of CYCs, but among these, the strong tidal fields play the most important role. Figure 7 compares the evolution of model 142 with a model which is the same in every respect, except that R_t is ten times larger (because the density profile is the same as in model 142, the cluster does not initially fill up the tidal radius in this case). Here, the effect of the tidal field is dramatically illustrated: when CYCs are located in tidal fields much weaker than in the GC, their lifetimes are several orders of magnitude longer. This could be the case for the R136 cluster in the LMC, which has cluster parameters similar to those of CYCs, but is apparently subjected to a much weaker tidal field.

5.2. Comparison with Observations

Of the Arches and Quintuplet clusters, the former is significantly more compact, and is estimated to be younger and more massive (see Table 2). The smaller central density of the Quintuplet may be due to an initial condition with lower concentration or smaller M than that of the Arches. However, because their ages are probably quite different, it is interesting to suppose that the two clusters had the same initial conditions and to see if they represent two distinct epochs in the evolutionary track of a cluster. Since the Arches is estimated to have $M = 1.2 \times 10^4 M_\odot$ and $R_g \sim 30$ pc, our models with $M = 2 \times 10^4 M_\odot$ and $R_g = 30$ pc can be considered to represent these clusters. Figure 8 shows the evolution of model 142, whose parameters are $M = 2 \times 10^4 M_\odot$, $\alpha = 2.35$, $W_0 = 4$, $R_g = 30$, and $m_l = 1 M_\odot$. By comparison with the locations of the clusters in this diagram, we infer that the Arches is located near the epoch of core collapse, and the Quintuplet is near the end of the evolution. Figure 8 lends plausibility to the idea that the two clusters started with the same initial conditions and that their largely different central densities are simply due to the age difference.

The two clusters may equally well be represented as different evolutionary stages of other model clusters having different values of α and m_l . Model 114, which has the same parameters as model 142 except for $\alpha = 2.5$, gives an evolutionary route similar to that of model 142, with a slightly longer t_{ev} . Meanwhile, smaller α values result in shorter t_{ev} , and smaller m_l values give longer t_{ev} . Thus clusters with an appropriate combination of smaller α and m_l will also be able to describe the two clusters together.

The mass function evolves due to mass segregation, selective ejection of lighter stars, and stellar evolution. Furthermore, the mass function varies with distance from the cluster center. Thus observations of the mass functions at several different radii, along with a determination of the cluster age, would all be needed to infer the cluster IMF. To illustrate this point, we present in Figure 9 the evolution of α for the whole cluster and for four equally-spaced annuli of model 142. Considering the observational inaccessibility of low mass stars, and the rapid evolution of massive stars, the determination of α was restricted to the mass range $[3, 30] M_\odot$. While the whole cluster mass function evolves relatively slowly until before the final disintegration phase, the mass function of each annulus evolves rather rapidly from the beginning. The differences in α values between annuli are largest near the core collapse. The α values of the outer annuli initially grow due to mass segregation, and later decrease as the tidal radius shrinks. Mass functions of CYCs measured with *HST* will soon be reported (Figer et al. 1999), and the radial dependence must clearly be considered. Since the mass function evolves from the very beginning, even the current mass function of the younger CYC, the Arches, will somewhat differ from the IMF.

The final disintegration of a cluster takes place in a relatively short period of time compared to the cluster's lifetime. Fukushige & Heggie (1995) argue that a cluster finally disrupts by losing equilibrium when R_h/R_t exceeds a certain critical value. At this point, the central density and velocity dispersion decrease abruptly, as may be seen in Figure 8. We find that our models have v_c less than or about 5 km s^{-1} only during the final disruption phase, before which clusters maintain v_c 's larger than or about 10 km s^{-1} . Therefore, an observation of v_c for the Quintuplet will be able to provide important information on the cluster's position in its evolutionary track.

If the Quintuplet is indeed in a disruption phase,

t_{ev} values calculated in this study may give a constraint on the initial condition of the cluster: the Quintuplet is not likely to initially have $\alpha \gtrsim 2.5$ if its m_l is as low as $0.1 M_\odot$, because the Quintuplet would not otherwise be in a disruption phase at its supposed current age.

5.3. The Star Formation Rate

The expected number of observed clusters at a certain epoch in the inner bulge, N_{obs} , is basically a function of M , t_{ev} , and the star formation rate (SFR) in the region:

$$N_{obs} = \int \int \frac{SFR}{M} t_{ev}(M, R_g) \phi(M, R_g) dR_g dM, \quad (15)$$

where $\phi(M, R_g)$ is a normalized probability that a cluster is formed with M at R_g . We assume initially that stars are all born in clusters. As shown in Figure 6, t_{ev} should apparently be dependent on both M and R_g . Thus here we adopt a simple, order-of-magnitude analysis for the relation between t_{ev} and N_{obs} . First we split the variables in t_{ev} and ϕ . For the former, we adopt a simple form,

$$t_{ev} = 3 \times 10^6 \text{ yr} \left(\frac{R_g}{30 \text{ pc}} \right)^{0.75} \left(\frac{M}{2 \times 10^4 M_\odot} \right). \quad (16)$$

The virtue of this approximation is that it, along with variable splitting for ϕ , makes equation (15) independent of M , whose distribution is not well known (in fact, the behaviour of t_{ev} 's is better described with $\propto M^{1/2}$ rather than $\propto M$, but we choose the latter for simpler estimation). For the latter, we define $\phi \equiv \phi_M(M) \phi_R(R_g)$, where ϕ_M and ϕ_R are normalized for their variables, and we assume that ϕ_R follows the density profile in the inner bulge ρ_g : $\phi_R \propto R_g^2 \rho_g \propto \text{const}$ ($\rho_g \propto R_g^{-2}$ is adopted instead of $\rho_g \propto R_g^{-1.8}$ for simplicity). We take $[0, 100]$ pc for the range of R_g (the final result is not so sensitive to the choice of this range). Then equation (15) now becomes

$$\begin{aligned} N_{obs} &\simeq 15 \left(\frac{SFR}{0.1 M_\odot \text{ yr}^{-1}} \right) \int_{0 \text{ pc}}^{100 \text{ pc}} \left(\frac{R_g}{30 \text{ pc}} \right)^{0.75} \\ &\quad \times \phi_R(R_g) dR_g \int \phi_M(M) dM \\ &\simeq 20 \left(\frac{SFR}{0.1 M_\odot \text{ yr}^{-1}} \right). \end{aligned} \quad (17)$$

N_{obs} is then equal to the actual current number of large, distinguishable clusters in the inner bulge, two,

if SFR is as low as $0.01 M_\odot \text{ yr}^{-1}$, a value which happens to be very close to the mass of the two clusters divided by their lifetime, which is a crude estimate of the SFR without any consideration of dependencies on R_g and M .

Güsten (1989) estimated the SFR in the inner bulge to be $0.3\text{-}0.6 M_\odot \text{ yr}^{-1}$ from the global production rate of Lyman continuum photons, and $0.05 M_\odot \text{ yr}^{-1}$ from the luminosity of the discrete far-IR sources measured by Odenwald & Fazio (1984). Güsten's estimates are based on the assumption of a Salpeter mass function with m_l of $0.1 M_\odot$. For a flatter mass function with elevated m_l , his SFR becomes smaller, although still considerably larger than $0.01 M_\odot \text{ yr}^{-1}$. It thus appears that a considerable fraction of stars in the inner bulge forms outside of clusters, or in much smaller clusters than the Arches and Quintuplet.

A number of other sites of star formation are known in the GC, but none apparently has a stellar luminosity within an order of magnitude of the Arches and Quintuplet. Partial surveys have been carried out at near-IR wavelengths to identify other potential clusters near the GC (Catchpole, Whitelock, & Glass 1990; Figer 1995; Philipp et al. 1999), but no others have yet been identified, and it seems likely that if there are any others comparable to the Arches or Quintuplet, they are highly obscured, even at 2 microns.

We therefore speculate that the circumstances of the formation of these clusters was peculiar in some fundamental way, such as catastrophic formation by extremely strong shocks, or direct collision of two dense molecular clouds. If so, then young stars near the GC are formed in multiple modes, and one cannot ascribe the total star formation rate there to massive clusters alone.

5.4. Binary Heating and Close Encounters

We find that in all of our models, heating by three-body binaries exceeds that by tidal-capture binaries during the core collapse, and that the postcollapse expansion is driven by three-body binaries. Moreover, in most models, the cumulative number of tidal binaries formed is less than unity until the end of evolution. These numbers are one to two orders of magnitude smaller than the number of collisional mergers between stars during the first few Myr calculated by Portegies Zwart et al. (1999) for the R136 cluster in the LMC with initial central mass density sim-

ilar to our models. The discrepancy is due to the fact that we did not consider the evolution of massive stars into a giant phase in which the stellar radii are largely increased. Thus our tidal-capture binary formation rates are somewhat underestimated, but since the heating per binary is much larger for three-body binaries, the inclusion of radius evolution into our calculations would not change the overall dynamical evolution of the clusters except only for some cases with considerably large initial central densities and steep IMFs (these conditions are more favorable to tidal-capture binary formation; see, e.g., Kim, Lee, & Goodman 1998). In these cases, the postcollapse expansion will be driven by tidal-capture binaries and clusters will expand more slowly than the ones driven by three-body binaries.

5.5. Dynamical Friction

Clusters are subject to dynamical friction as they go through field stars while orbiting around the galaxy center. The drag by dynamical friction causes the clusters to lose energy and spiral in toward the center, where the tidal field is stronger. When the field stars have a density distribution $\propto R_g^{-2}$, the time required for a cluster initially on a circular orbit to reach the center is given by

$$t_{fric} \simeq \frac{2 \times 10^9 \text{ yr}}{\ln \Lambda} \left(\frac{R_g}{30 \text{ pc}} \right)^2 \left(\frac{M}{2 \times 10^4 M_\odot} \right)^{-1} \left(\frac{v_c}{170 \text{ km s}^{-1}} \right), \quad (18)$$

where v_c is the circular orbital velocity of the cluster and $\ln \Lambda$ is the Coulomb logarithm for the field stars (Binney & Tremaine 1987). Reasonable values for the inner bulge are $v_c \simeq 170 \text{ km s}^{-1}$ and $\ln \Lambda \approx 10$. Then t_{fric} would be comparable to or smaller than t_{ev} calculated in this study only for clusters with extremely small R_g and/or large M . Thus, most CYCs will disintegrate through tidal evaporation before a significant orbital decay due to dynamical friction takes place.

5.6. Limitations

We assumed that clusters consist of coevally formed stars and start their main-sequence stages at the beginning of simulations. However, stars may gravitationally interact with others already from pre-main-sequence or even from accreting protostar stages and these stages may be important to CYCs because of

their short t_{ev} 's. For very massive stars, the time scale of these stages prior to the main-sequence must be much shorter than t_{ev} 's calculated in this study, but it becomes larger than 10 Myr for stars lighter than $2 M_\odot$ (Bernasconi 1996). Thus if lighter stars systematically form earlier than heavier stars, the dynamical evolution of lighter stars until the formation of heavier stars may become important. The role of the stages prior to main-sequence on the cluster's lifetime is not clear though, because not much is yet known about the details of cluster formation, such as what fraction of the gas goes into star formation (star formation efficiency), how quickly the gas left over from star formation disappears from the cluster by stellar wind and supernova explosions (timescale of residual gas expulsion), and which gas clumps (as a function of mass) contract into stars first and act as discrete gravity sources. These uncertainties are particularly large for the unusual clusters we are considering here. These issues are in the arena of N-body simulations and the first two issues were considered by Tenorio-Tagle et al. (1986) and Goodwin (1997a,b) for young globular clusters. No observational evidence for the presence of residual gas in the Arches and Quintuplet has been found yet. Proper inclusion of these effects into early cluster dynamics will be possible only after a significant advance in the study of star formation is achieved.

Throughout the calculations, we have set $N_{15} = 50$, but this value is arbitrarily chosen. Higher values would give more statistically correct results, but would not represent the whole mass range well. This is one of the intrinsic limitations with Fokker-Planck simulations. To see the dependence of t_{ev} on N_{15} , we performed models 142 and 145 with $N_{15} = 150$, and obtained only $\sim 25\%$ larger t_{ev} values. This implies that the choice of N_{15} does not significantly alter our general results. On the other hand, our single-power-law IMFs may be too simple to represent realistic IMFs. Thus we tried a Kroupa IMF (Kroupa, Tout, & Gilmore 1993), which is a three-part power-law with $\alpha = 2.7$ for $m > 1 M_\odot$, 2.2 for $0.5 M_\odot < m < 1 M_\odot$, and 1.3 for $0.08 M_\odot < m < 0.5 M_\odot$, for $M = 2 \times 10^4 M_\odot$, $R_g = 30 \text{ pc}$, and $W_0 = 4$. We found that the model with a Kroupa IMF has results similar to those of model 116, in which the parameters are $\alpha = 2.5$ and $m_l = 0.1 M_\odot$. Since the Kroupa IMF was derived for the Galactic disk, it may not be applicable to the GC where the star formation environment is largely different from that in the disk, but

we believe that even the evolution of a cluster with realistic GC IMF can be well approximated with one of our simple power-law IMFs.

Orbit-averages used in our Fokker-Planck simulations are valid when $t_{dyn} \ll t_{rh}$. Since $t_{rh} \approx (0.1N/\ln \Lambda)t_{dyn}$, CYCs, which have N of $\sim 10^{3-5}$, apparently satisfy the requirement. However, the wide mass range of CYCs shortens the relaxation time in the core through mass segregation, and the above requirement may not hold in the core for some of our models, especially the ones with the largest mass ranges. In addition, while the Fokker-Planck method also assumes $t_{dyn} \ll t_{se}$, some of our models with large M and small α may have periods when the assumption is temporarily violated. The validity of using the Fokker-Planck method for these marginal situations can be assessed using N-body simulations.

6. SUMMARY

We have investigated the dynamical evolution of CYCs near the Galactic center with anisotropic Fokker-Planck models. Stellar evolution and heating by three-body and tidal-capture binaries were included in the calculation, and the apocenter criterion with an appropriate removal speed constant was adopted for the tidal evaporation. Mass bins were chosen depending on cluster parameters to properly account for a relatively small number of most massive stars.

The evolutionary time scales of CYCs are fairly short because of their compactness and strong tidal fields. For our parameter regime ($1.5 \leq \alpha \leq 2.5$, $m_l = 0.1 \text{ \& } 1 M_\odot$, $5 \times 10^3 M_\odot \leq M \leq 10^5 M_\odot$, and $10 \text{ pc} \leq R_g \leq 100 \text{ pc}$), clusters evaporate in $\lesssim 10$ Myr except for few clusters with $M = 10^5 M_\odot$. Core collapse takes place in most clusters, and three-body binaries dominate the heating.

Unlike globular clusters, very massive stars in CYCs play important roles in dynamics because relaxation and mass segregation times are comparable to or even smaller than those stars' lifetimes. Rapid mass segregation due to a large difference in upper and lower mass boundaries accelerates a cluster's evolution even more. Strongly selective ejection of lighter stars makes massive stars dominate even in the outer regions of the cluster and the evolution of such clusters is weakly dependent on the lower mass boundary.

We found that the Arches and Quintuplet clusters, which have quite different central densities, central concentrations, and ages, may be placed on one evo-

lutionary track. Among our cluster models, that with $M = 2 \times 10^4 M_\odot$, $R_g = 30 \text{ pc}$, $\alpha = 2.35$ or 2.5 , and $m_l = 1 M_\odot$ gives the evolutionary track that best describes both clusters simultaneously. The first two parameters are from observational constraints, and an appropriate combination of smaller α and m_l can also describe the two clusters together.

The total mass in observed CYCs is several $10^4 M_\odot$ and the lifetime of CYCs with observed M at observed R_g is a few Myr. These numbers result in an inner bulge SFR of $\sim 0.01 M_\odot \text{ yr}^{-1}$. A more detailed (but still approximate) estimate of the SFR with a consideration of distributions in M and R_g happens to be similar to this simple estimate. Lyman continuum photons and far-IR observations in the inner bulge region give SFRs of $0.05\text{--}0.5 M_\odot \text{ yr}^{-1}$. We suggest that the mode of formation of CYCs is peculiar, likely resulting from strong shocks or collisions of dense molecular clouds.

S.S.K. is deeply grateful to Koji Takahashi for generously providing us of his anisotropic Fokker-Planck codes and for his kind help with the codes. We thank Don Figer, Cheongho Han, Eunhyeuk Kim, Pavel Kroupa, Myung Gyoon Lee, Kap Soo Oh, R. Michael Rich, and Rainer Spurzem for helpful discussions. This work was supported in part by the International Cooperative Research Program of the Korea Research Foundation to Pusan National University in 1998, and in part by NASA through grant number GO-07364.01-96A to UCLA from the Space Telescope Science Institute, which is operated by AURA, Inc., under NASA contract NAS5-26555.

REFERENCES

- Aarseth, S. J., & Heggie, D. C. 1998, MNRAS, 297, 794
- Bahcall, J. N., & Wolf, R. A. 1977, ApJ, 216, 883
- Bernasconi, P. A. 1996, A&AS, 120, 57
- Binney, J., & Tremaine, S. 1987, Galactic Dynamics (Princeton: Princeton Univ. Press)
- Catchpole, R. M., Whitelock, P. A., & Glass, I. S. 1990, MNRAS, 247, 479
- Chernoff, D. F., & Weinberg, M. D. 1990, ApJ, 351, 121
- Cohn, H. 1985, in IAU Symp. 113, Dynamics of Star Clusters, eds. J. Goodman & P. Hut (Dordrecht: Reidel), 161

- Cotera, A. S., Erickson, E. F., Colgan, S. W. J., Simpson, J. P., & Allen, D. A. 1996, *ApJ*, 461, 750
- Drukier, G. A. 1995, *ApJS*, 100, 347
- Figer, D. F. 1995, PhD Thesis, Univ. of California, Los Angeles
- Figer, D. F., McLean, I. S., & Morris, M. 1995, *ApJ*, 447, L29
- Figer, D. F., McLean, I. S., & Morris, M. 1999, *ApJ*, in press
- Fukushige, T., & Heggie, D. C. 1995, *MNRAS*, 276, 206
- Gaume, R. A., Claussen, M. J., De Pree, C. G., Goss, W. M., & Mehringer, D. M. 1995, *ApJ*, 449, 663
- Genzel, R., & Townes, C. H. 1987, *ARAA*, 25, 377
- Glass, I. S., Moneti, A., & Moorwood, A. F. M. 1990, *MNRAS*, 242, 55p
- Goodwin, S. P. 1997a, *MNRAS*, 284, 785
- Goodwin, S. P. 1997b, *MNRAS*, 286, 669
- Güsten, R. 1989, in *IAU Symp. 136, The Center of the Galaxy*, ed. M. Morris (Dordrecht: Kluwer), 89
- Hénon, M. 1961, *Ann. Astrophys.*, 24, 369
- Ho, L. C., & Filippenko, A. V. 1996, *ApJ*, 472, 600
- Kim, S. S., & Lee, H. M. 1999, *A&A*, in press
- Kim, S. S., Lee, H. M., & Goodman, J. 1998, 495, 786
- Kroupa, P., Tout, C. A., & Gilmore, G. 1993, *MNRAS*, 262, 545
- Lee, H. M., Fahlman, G. G., & Richer, H. B. 1991, *ApJ*, 366, 455
- Lee, H. M., & Goodman, J. 1995, *ApJ*, 443, 109
- Lee, H. M., & Ostriker, J. P. 1987, *ApJ*, 322, 123
- Lee, H. M., & Ostriker, J. P. 1993, *ApJ*, 409, 617
- Lindqvist, M., Habing, H. J., & Winnberg, A. 1992, *A&A*, 259, 118
- Morris, M. 1993, *ApJ*, 408, 496
- Nagata, T., Woodward, C. E., Shure, M., Pipher, J. L., & Okuda, H. 1990, *ApJ*, 351, 83
- Nagata, T., Woodward, C. E., Shure, M., & Kobayashi, N. 1995, *AJ*, 109, 1676
- Odenwald, S. F., & Fazio, G. G. 1984, *ApJ*, 283, 601
- Okuda, H., Shibai, H., Nakagawa, T., Matsuhara, H., Kobayashi, Y., Kaifu, N., Nagata, T., Gatley, I., & Geballe, T. R. 1990, *ApJ*, 351, 89
- Philipp, S., Zylka, R., Mezger, P. G., Duschl, W. J., Herbst, T., & Tuffs, R. J. 1999, *A&A*, submitted
- Portegies Zwart, S. F., Hut, P., Makino, J., & McMillan, S. L. W. 1998, *A&A*, 337, 363
- Portegies Zwart, S. F., Makino, J., McMillan, S. L. W., & Hut, P. 1999, *A&A*, submitted
- Schaller, G., Schaerer, D., Meynet, G., & Maeder, A. 1992, *A&AS*, 96, 269
- Serabyn, E., & Morris, M. 1995, *Nature*, 382, 602
- Serabyn, E., Shupe, D., & Figer, D. F. 1998, *Nature*, 394, 448
- Sjouwerman, L. O., Habing, H. J., van Langevelde, H. J., & Winnberg, A. 1998, in *IAU Symp. 184: The Central Region of the Galaxy and Galaxies*, ed. Y. Sofue (Dordrecht: Kluwer), 67
- Takahashi, K. 1997, *PASJ*, 49, 547
- Takahashi, K., Lee, H. M., & Inagaki, S. 1997, *MNRAS*, 292, 331
- Takahashi, K., & Portegies Zwart, S. F. 1998, *ApJ*, 503, L49
- Tenorio-Tagle, G., Bodenheimer, P., Lin, D. N. C., & Noriega-Crespo, A. 1986, *MNRAS*, 221, 635

TABLE 1
SIMULATION PARAMETERS AND RESULTS

Models	α	W_0	M (M_\odot)	R_g (pc)	R_t (pc)	$m_l - m_u$ (M_\odot)	β	\bar{m} (M_\odot)	m_{15} (M_\odot)	t_{ev} (Myr)
101	2	4	2×10^4	30	1.11	1-150	0.526	5.04	84.3	2.7
102	2	4	2×10^4	30	1.11	0.1-150	0.722	0.73	72.1	2.9
103	2	4	2×10^4	30	1.11	1-75	0.659	4.37	54.9	4.0
111	2	1	2×10^4	30	1.11	1-150	0.526	5.04	84.3	2.7
112	2	7	2×10^4	30	1.11	1-150	0.526	5.04	84.3	2.7
113	1.5	4	2×10^4	30	1.11	1-150	0.266	12.25	111.6	2.3
114	2.5	4	2×10^4	30	1.11	1-150	0.763	2.76	49.5	5.1
115	1.5	4	2×10^4	30	1.11	0.1-150	0.430	3.87	109.9	2.2
116	2.5	4	2×10^4	30	1.11	0.1-150	1.000	0.29	26.7	11.2
117	2	1	2×10^4	30	1.11	0.1-150	0.722	0.73	72.1	2.8
118	2	7	2×10^4	30	1.11	0.1-150	0.722	0.73	72.1	2.8
121	1.5	4	1×10^5	30	1.89	1-150	0.966	12.25	140.3	3.0
122	2	4	1×10^5	30	1.89	1-150	1.020	5.04	127.3	4.1
123	2.5	4	1×10^5	30	1.89	1-150	1.124	2.76	92.9	15.8
124 ^a	1.5	4	5×10^3	30	0.70	1-150	...	12.25	62.4	1.2
125	2	4	5×10^3	30	0.70	1-150	0.108	5.04	42.7	1.6
126	2.5	4	5×10^3	30	0.70	1-150	0.384	2.76	24.2	2.4
127	2	4	1×10^5	30	1.89	0.1-150	1.032	0.73	119.5	4.8
128	2.5	4	1×10^5	30	1.89	0.1-150	1.184	0.29	59.3	75.5
129	2	4	5×10^3	30	0.70	0.1-150	0.506	0.73	33.9	1.8
130	2.5	4	5×10^3	30	0.70	0.1-150	0.828	0.29	12.0	4.8
131	2	4	5×10^3	10	0.36	1-150	0.108	5.04	42.7	0.6
132	2	4	2×10^4	10	0.57	1-150	0.526	5.04	84.3	1.1
133	2	4	1×10^5	10	0.98	1-150	1.020	5.04	127.3	2.7
134	2	4	5×10^3	100	1.43	1-150	0.108	5.04	42.7	4.1
135	2	4	2×10^4	100	2.28	1-150	0.526	5.04	84.3	4.9
136	2	4	1×10^5	100	3.89	1-150	1.020	5.04	127.3	7.6
141	2.35	4	5×10^3	30	0.70	1-150	0.306	3.19	29.0	2.2
142	2.35	4	2×10^4	30	1.11	1-150	0.691	3.19	59.4	4.0
143	2.35	4	1×10^5	30	1.89	1-150	1.083	3.19	105.6	8.6
144	2.35	4	5×10^3	30	0.70	0.1-150	0.735	0.36	16.9	3.3
145	2.35	4	2×10^4	30	1.11	0.1-150	0.913	0.36	37.6	6.4
146	2.35	4	1×10^5	30	1.89	0.1-150	1.122	0.36	79.3	40.8
151	2.35	4	5×10^3	10	0.36	1-150	0.306	3.19	29.0	0.8
152	2.35	4	2×10^4	10	0.57	1-150	0.691	3.19	59.4	1.5
153	2.35	4	1×10^5	10	0.98	1-150	1.083	3.19	105.6	4.0
154	2.35	4	5×10^3	100	1.43	1-150	0.306	3.19	29.0	6.5
155	2.35	4	2×10^4	100	2.28	1-150	0.691	3.19	59.4	12.0
156	2.35	4	1×10^5	100	3.89	1-150	1.083	3.19	105.6	24.2

^a β becomes a negative value for this model, so an equal logarithmic binning was used instead.

TABLE 2
 PROPERTIES OF COMPACT YOUNG CLUSTERS

Cluster	Log M (M_{\odot})	R_{av} (pc)	Log ρ_{av} ($M_{\odot} \text{ pc}^{-3}$)	Age (Myr)
Arches	4.3	0.2	5.8	1-2
Quintuplet	3.8	1.0	3.2	3-5
R136	4.5	1.6	3.3	< 1 – 2

NOTE.—From Table 5 of Figer et al. (1999). M is the total cluster mass in all stars extrapolated from observation down to a lower-mass cutoff of $1 M_{\odot}$, assuming a Salpeter IMF slope and an upper mass cutoff of $120 M_{\odot}$. R_{av} is the average projected separation from the centroid position. Since the low-mass end has not been identified in these clusters yet, the radius may be larger than the value given here when mass segregation is present. ρ_{av} is M divided by the volume inside R_{av} .

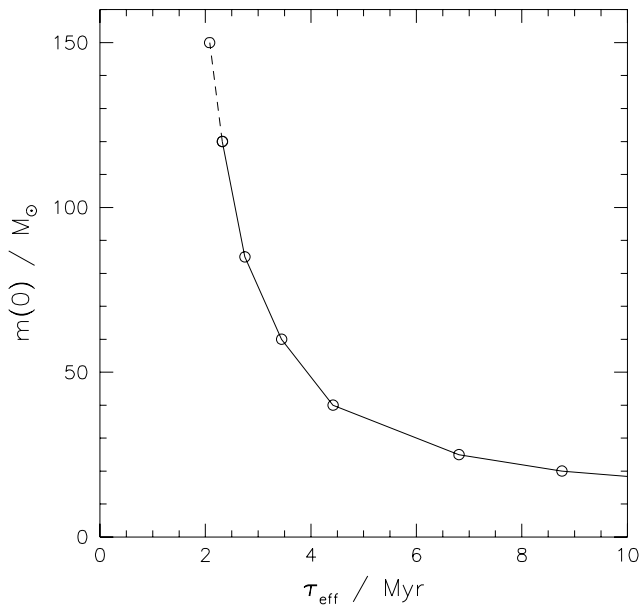


Fig. 1.— The effective lifetime τ_{eff} of a star with initial mass $m(0)$ defined by equation (9). Schaller et al. (1992) was adopted for $m(t)$. A logarithmic extrapolation has been made for $m(0) > 120 M_{\odot}$. These τ_{eff} values are used for $\tau_{i \pm \frac{1}{2}}$ in equation (8).

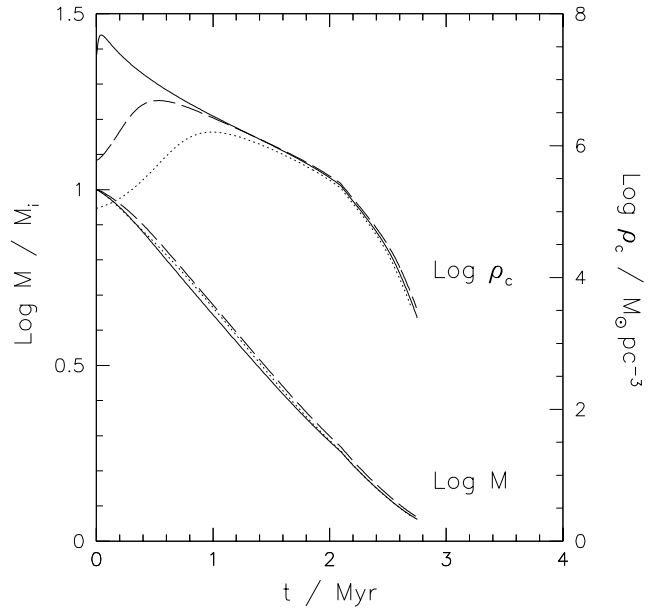


Fig. 2.— Evolution of M and ρ_c for models 111 ($W_0 = 1$; dotted lines), 101 ($W_0 = 4$; dashed lines), and 112 ($W_0 = 7$; solid lines), which have the same initial conditions except for W_0 . These models have largely different t_{cc} but very similar t_{ev} . This shows that t_{ev} is independent of W_0 .

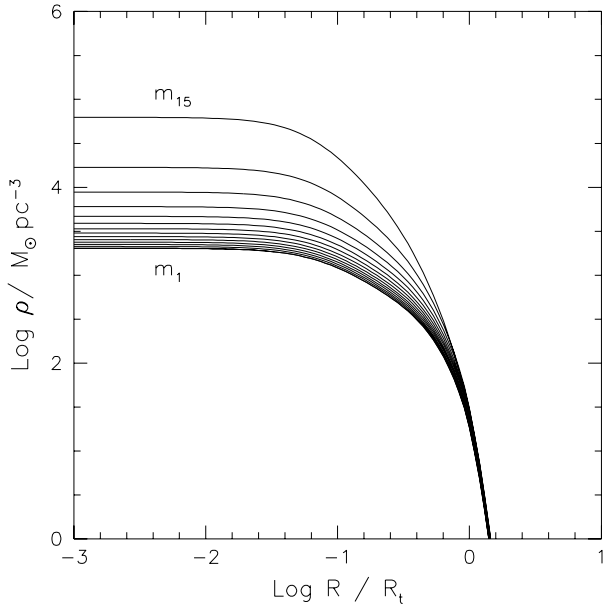


Fig. 3.— Density profiles of mass component 1 to 15 (bottom to top) of model 142 at $t = 2$ Myr (post-collapse phase). Both core and envelope are dominated by heavy components.

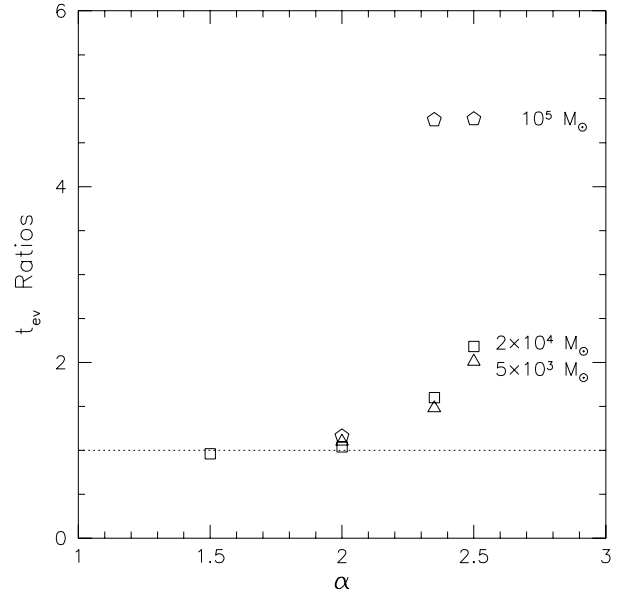


Fig. 4.— The ratios of t_{ev} between models with the same parameters except m_l (t_{ev} for $m_l = 0.1 M_\odot$ over t_{ev} for $m_l = 1 M_\odot$). Models shown here have $R_g = 30$ pc and $W_0 = 4$. Triangles are for $M = 5 \times 10^3 M_\odot$, squares for $M = 2 \times 10^4 M_\odot$, and pentagons for $M = 10^5 M_\odot$. The dotted line represents t_{ev} ratios of unity. For $\alpha \lesssim 2$, t_{ev} is nearly independent of m_l in range $0.1 < m_l / M_\odot < 1$. For $M \lesssim 2 \times 10^4 M_\odot$, t_{ev} differs only by a factor of $\lesssim 2$ up to $\alpha = 2.5$ in the same m_l range.

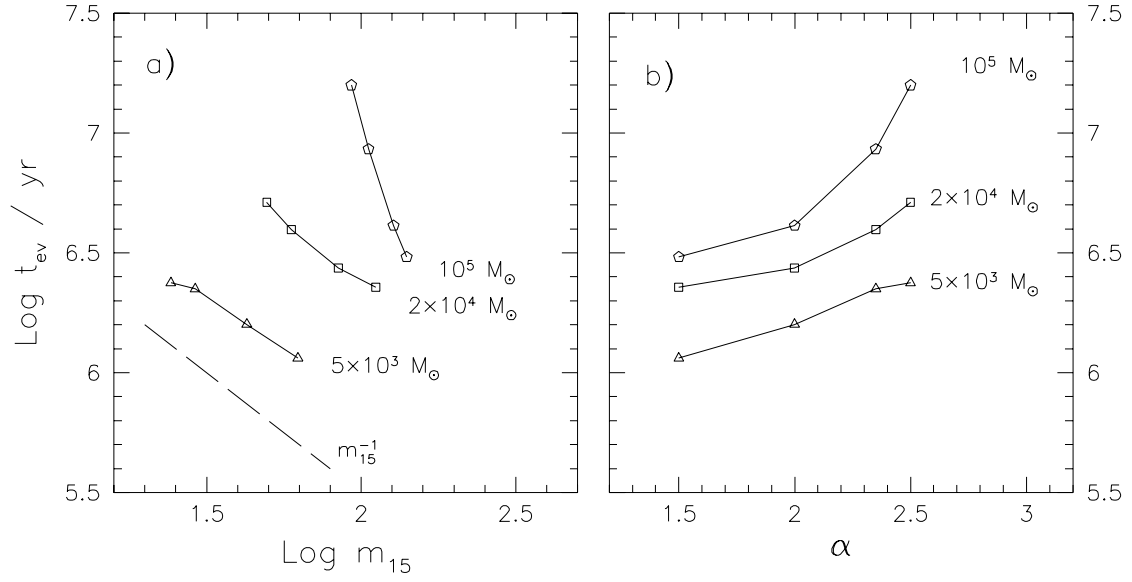


Fig. 5.— t_{ev} as a function of m_{15} (a) and α (b) for models with $m_l = 1 M_\odot$ and $R_g = 30 \text{ pc}$, and $W_0=4$. Symbols are the same as in Figure 4. Dashed line represents $t_{ev} \propto m_{15}^{-1}$ relation.

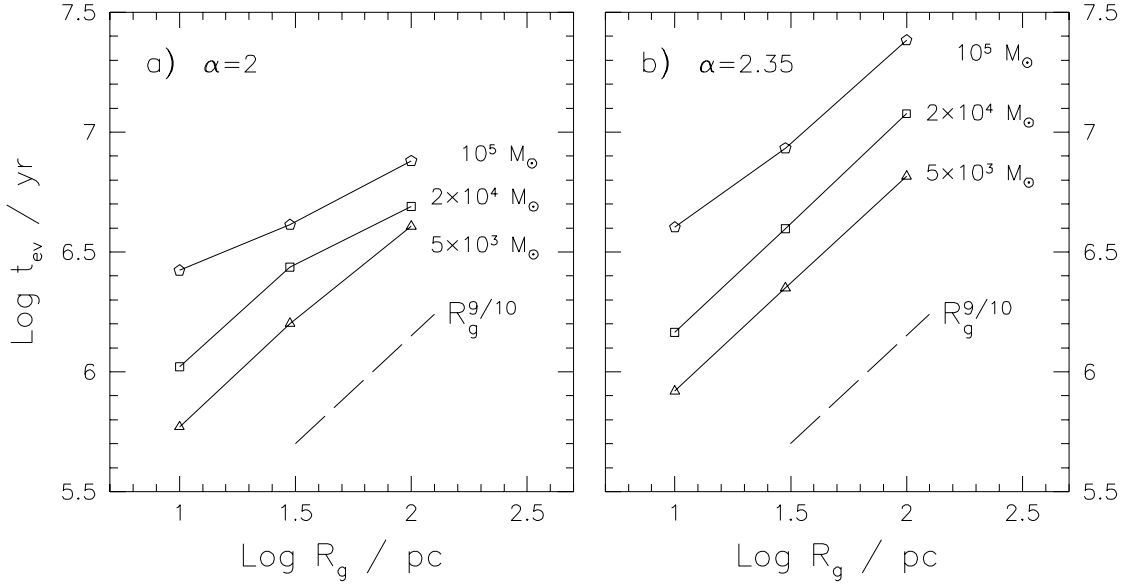


Fig. 6.— t_{ev} as a function of R_g for models with $m_l = 1 M_\odot$, $W_0 = 4$, and $\alpha = 2$ (a) and 2.35 (b). Symbols are the same as in Figure 4. Without stellar evolution, $t_{ev} \propto R_g^{9/10}$ (dashed lines) would be expected.

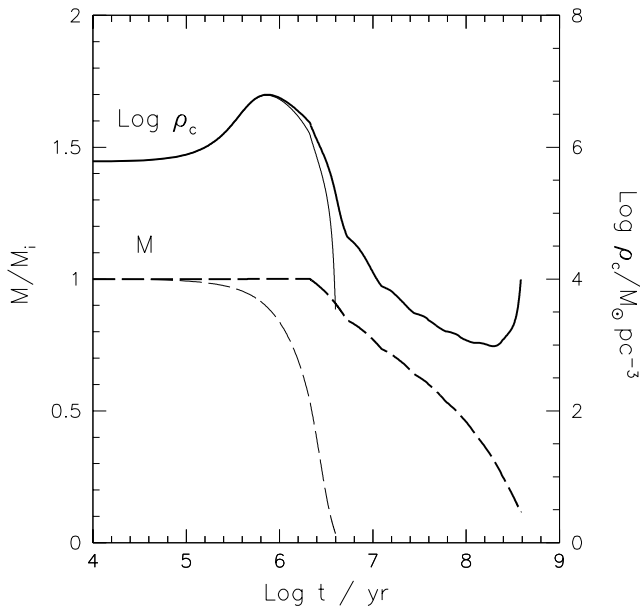


Fig. 7.— ρ_c (solid lines) and M (dashed lines) evolution of model 142 (thin lines) and the same model with a ten times larger R_t (thick lines). The density profile of the latter is set to be the same as the former, so the cluster of the latter model does not initially fill up the tidal radius. This figure clearly shows the effects of strong tidal fields on t_{ev} . The ρ_c of the model with a ten times larger R_t has a second core collapse at the end of the evolution.

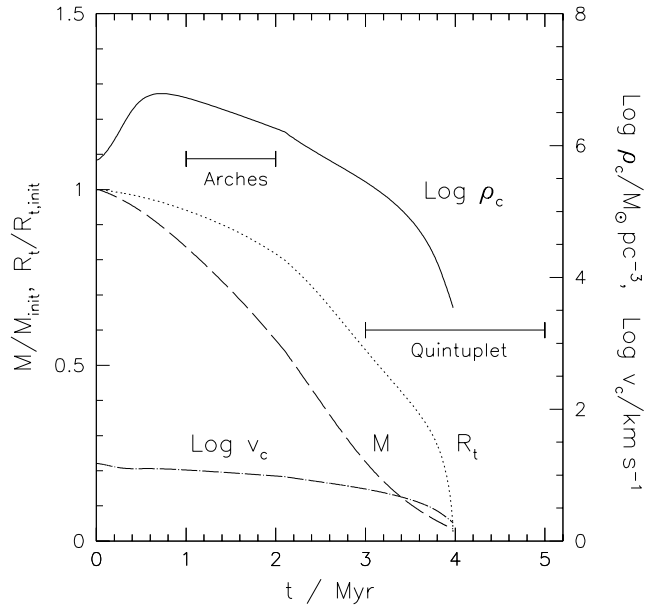


Fig. 8.— Evolution of ρ_c (solid line), M (dashed line), R_t (dotted line), and v_c (dash-dotted line) of model 142. M and R_t are normalized with their initial values. The estimated locations in t - ρ_{av} plane for the Arches and Quintuplet clusters are indicated with bars (data from Table 2; note that ρ_c 's of the clusters will be slightly higher than ρ_{av} especially for the Arches which shows a high central concentration). The Arches, the more compact of the two, is situated near the epoch of core collapse, and the Quintuplet, which looks much less bound, corresponds to the final disruption phase of model 142. The Figure may imply that two clusters had similar initial conditions, and represent two distinctly different epochs in their evolution.

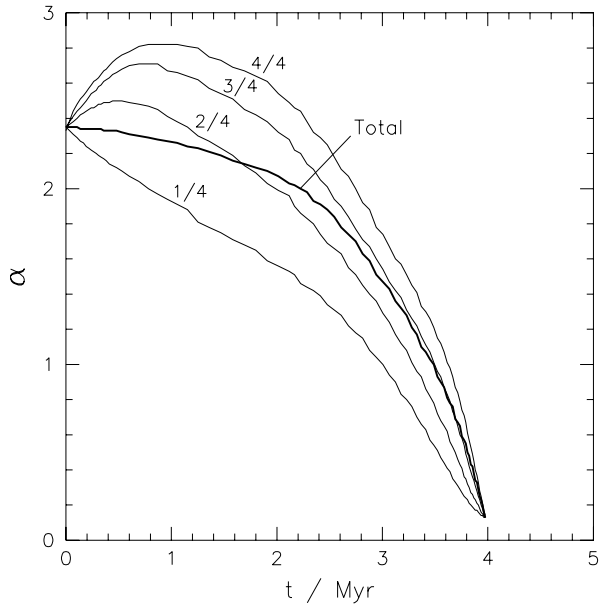


Fig. 9.— Evolution of α for the whole cluster (thick line) and four inner-to-outer, equally-spaced annuli between the center and R_t (thin lines; from bottom to top) of model 142. Considering the lower detection limit in observations and stellar evolution of massive stars, α was obtained for the mass range of $[3, 30] M_{\odot}$.